Soft Matter

Accepted Manuscript

This is an *Accepted Manuscript*, which has been through the Royal Society of Chemistry peer review process and has been accepted for publication.

Accepted Manuscripts are published online shortly after acceptance, before technical editing, formatting and proof reading. Using this free service, authors can make their results available to the community, in citable form, before we publish the edited article. We will replace this *Accepted Manuscript* with the edited and formatted *Advance Article* as soon as it is available.

You can find more information about *Accepted Manuscripts* in the **Information for Authors**.

Graphical abstract:

Two-dimensional SAXS patterns reveal deformation and re-orientation of microdomains in a hexagonally ordered block copolymer melt subjected to uniaxial extensional flow.
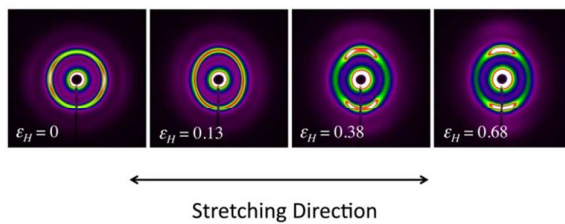
Structural response of an ordered block copolymer melt to uniaxial extensional flow

Ruinan Mao, Erica M. McCready and Wesley R. Burghardt*

Department of Chemical and Biological Engineering

Northwestern University

Evanston, IL 60208

* Corresponding author: w-burghardt@northwestern.edu

Abstract

We report *in situ* small-angle x-ray scattering (SAXS) studies of a cylindrically ordered styrene-ethylene butylene-styrene (SEBS) triblock copolymer melt subjected to uniaxial extensional flow. The flow is applied by stretching strips of polymer melt using a counter-rotating drum extensional flow fixture housed in a custom oven designed to provide x-ray access. SAXS patterns show two distinct modes of structural response during extensional flow: deformation of the microscopic structure, and re-orientation of PS microdomains towards the flow direction. The *d*-spacings of the hexagonally ordered domains measured parallel and perpendicular to the flow direction deform affinely until Hencky strains of ~ 0.2. Departures in extensional viscosity from linear viscoelastic predictions are observed at similar strain. The azimuthal dependence of the primary diffraction peak reveals a complex re-orientation process whereby PS microdomains rotate toward the stretching direction. At intermediate strains, a '4-point' diffraction pattern indicates the presence of two discrete populations of microdomain orientation, attributed to a buckling instability of microdomains initially oriented perpendicular to the stretching direction. Flow-induced deformation and orientation both relax upon cessation of flow, albeit at very different rates, suggesting that these two modes of structural response are largely decoupled.

Introduction

Self-assembly via microphase separation in block copolymers (BCPs) is a powerful route to nanostructured materials.[1] Further, extensive research has documented the ability of shear flows to impart macroscopic alignment of ordered microdomains in block copolymer melts, and the role of various dynamic & topological features in directing transient alignment trajectories.[2,3] Comparatively little attention, however, has been paid to the response of ordered BCP melts to extensional flows, and very few efforts have been made in the realm of structural studies *during* extensional flow. There have been numerous examples of coordinated mechanical/structural testing in *solid* BCP samples at room temperature, where complications of temperature control and chain relaxation dynamics in the melt state are avoided. In particular, synchrotron x-ray scattering studies of BCP-based thermoplastic elastomers have enabled detailed investigation of structural changes that provide insight into the macroscopic material behavior.[4-6] Our objective here is to apply similar methodology to study the structural response of an ordered BCP *melt* to a well-defined uniaxial extensional flow.

Abundant evidence of the ability to orient BCP melts in extension comes from observations of macroscopic alignment of both lamellar[7] and cylindrical[8-10] microphase separated melts during planar squeezing flows. The primary emphasis of these studies was the preparation of oriented samples for subsequent solid-state mechanical or melt rheological testing. Thus, the flow kinematics were not well defined, only limited efforts were made to vary deformation rates, and there was no possibility to study the orientation dynamics within the melt phase during the applied deformation. More recently, there have been several studies of BCP melts under better-defined rheometric conditions using

3

Meissner-type[11] uniaxial extensional rheometers. In some cases, only the mechanical response has been measured, and data analyzed in the context of continuum viscoelastic models with no complementary structural characterization.[12] Closer to the goals of the present work is a series of studies by Kotaka and Okamoto and coworkers, again using a Meissner rheometer that was modified to facilitate *in situ* rheo-optical birefringence measurements.[13-16] In addition to on-line birefringence, samples were also quenched at various points during elongation to allow *ex situ* SAXS characterization. These methods have been applied to block copolymers with spherical,[13] cylindrical[14,15] and lamellar[16] microdomains. While these studies provide insights into BCP structural evolution under controlled uniaxial flow, they also illustrate the limitations imposed by available instrumentation. The *in situ* birefringence data suffer from ambiguities associated with multiple optical retardation orders, while *ex situ* SAXS from quenched samples allows for only a few 'snapshots' of structure during deformation, and are inevitably subject to concerns about structural changes during sample quenching.

While extension can clearly promote alignment of BCP melts, brief reflection reveals that ordered block copolymer phases will be subjected to severe duress by such deformations. The most basic difference between shear and extension is that no alignment state exists in a uniaxial extensional deformation where an ordered BCP can avoid deformation, be it compression or expansion of the underlying microphase-separated morphology. In addition to revealing details of the alignment trajectories during extensional flow, *in situ* SAXS investigations can provide deeper insights into local structure (e.g. anisotropic changes in Bragg spacing) than are possible using the *ex situ* methods that have been available to date.

4

Structural studies of polymer melts in extensional flow first require a device capable of producing the desired flow in a controlled way, a long-standing challenge in rheometry. One classic strategy is, essentially, to perform a tensile test on a cylindrical melt sample, in which an exponential stretching of sample length is employed to impose a constant extension rate. Such methods were pioneered by Munstedt and Laun,[17,18] and are currently employed in melt extensional viscosity measurements using 'filament stretching' rheometers.[19,20] However, the size and operational complexity of these instruments would present considerable difficulties in a synchrotron environment. A second successful strategy for melt extensional rheometry was introduced by Meissner,[11,21] in which strips of polymer melt are stretched between counter-rotating clamps. The same principle provides the foundation for the more recently introduced extensional flow device used in the present work, the Sentmanat Extensional Rheometer (SER) fixture,[22,23] which is widely available commercially as an accessory for conventional rotational rheometers. Relative to the original Meissner design, the SER fixture has a more restricted range of total deformation that may be applied, and the use of wider and shorter sample strips raises concerns of imperfect uniaxial flow kinematics.[24] However, the sample configuration in the SER fixture is ideally suited for adaptation for *in situ* scattering measurements.

Experimental section

Materials

This study employs a triblock copolymer (SEBS) with styrene end blocks and a mid block of ethylene-butylene rubber. The copolymer sample was donated by Kraton polymers, with a reported molecular weight of 87,000 and styrene content of 13 wt%.

This polymer closely resembles a material studied extensively by Modi and coworkers,[25] who reported an order-disorder transition (ODT) at approximately 190°C, and the existence of an order-order transition (OOT) between cylindrical and spherical microdomain structures at approximately 140°C. Of these two domain structures, Modi *et al.* report that cylindrical ordering readily forms upon quenching disordered samples below the OOT, but that the sample will undergo a slow transition to spherical domain ordering when annealed at temperatures above the OOT. The exact microphase separated structure in this sample can thus potentially be a function of thermal history. As discussed below, we have confirmed that the sample studied here conforms in all respects to the behavior reported by Modi et al.[25]

In order to fully erase prior processing history, pellets of the SEBS copolymer were first dissolved in toluene and the polymer was cast roughly into films via solvent evaporation. These films were held in a vacuum oven at elevated temperatures to ensure complete removal of the solvent. The polymer was next compression molded into sheets of thickness of approximately 0.8 mm. The molding protocol included an initial period at 200°C for 20 minutes, followed by 8 hours of annealing at 130°C. Extended annealing at 130°C should result in local hexagonal ordering of cylindrical polystyrene microdomains with a globally random 'grain' orientation distribution owing to the initial molding step above the ODT. SAXS data presented below confirm hexagonal ordering. For testing in extensional flow, these sheets were then cut into sample strips 9 mm wide and 22 mm long. The same thermal protocol was used to compression mold sample disks for conventional linear viscoelastic characterization in shear.

Rheometry

Rheological testing was performed using an ARES-LS controlled strain rheometer (Rheometrics Scientific). Most testing was performed in the melt at a temperature of 130˚C. Additional tests were performed at other temperatures to confirm similarities to previous literature reports of rheological and phase behavior.[25] Testing at temperatures above 150˚C was performed under an inert nitrogen atmosphere. Linear viscoelastic characterization using oscillatory shear flow employed 25 mm diameter parallel plate fixtures. Measurements of transient uniaxial viscosity were performed using an SER extensional flow fixture. Full details of the principle of operation of the SER fixture are available elsewhere.[22,23] In brief, strips of sample are stretched between small counter-rotating drums driven at constant angular velocity by the rheometer's motor. The tensile force in the stretching polymer melt sample results in a torque that is measured by the rheometer's transducer. Tensile force data are converted to true stress by dividing by the exponentially decreasing sample cross-sectional area, and then to extensional viscosity by dividing by the applied extension rate. Extensional flow conditions used in mechanical rheometry were chosen to match those used for *in situ* structural tests. Given limitations in the x-ray data acquisition rate (details below), relatively small extension rates ranging from 0.01 to 0.05 s^{-1} were used to allow adequate time/strain resolution as samples were stretched to a final Hencky strain of 2.5. [Hencky strain, a measure of the total deformation in uniaxial extensional flow, is given by the product of extension rate and time: $\varepsilon_H = \dot{\varepsilon}t$. The total final stretch ratio $l/l_0 = \exp(\varepsilon_H)$ is equal to 12.2 in these experiments, corresponding to an engineering strain of 1120%.]

7

To assess the quality of the extensional flow kinematics produced by the SER, a series of samples were stretched to various final strains in off-line experiments, and the changes in sample dimensions produced by the flow were measured. Over the entire range of strain studied, uniaxial deformation was observed. That is, the fractional reductions in the width and the thickness of the sample were the same. However, for Hencky strains of ~ 1 and above, the final sample cross sectional area was smaller than expected based on the programmed strain. This means that, in the late stages of these experiments, (i) the actual strain experienced by the sample exceeds the nominal strain, and (ii) the actual extension rate exceeds the nominal extension rate. Effects of negative deviations in sample cross section and positive deviations in extension rate should cancel to some extent in calculation of extensional viscosity. However, these non-idealities do create uncertainty in the reported extensional viscosity values during the later stages of experiments.

X-ray scattering

Small-angle x-ray scattering was used to study the structural response of the SEBS triblock copolymer melt during uniaxial extensional flow. These experiments utilized an instrument in which the SER fixture is incorporated into a home-built convection oven designed to provide access of incident and scattered x-ray beams to and from the deforming sample. Specifically, the incident x-ray beam is passed between the two cylindrical drums of the SER fixture and through the deforming strip of polymer melt. In this instrument the SER fixture is driven by a stepper motor, and there were no provisions for simultaneous torque measurement during the SAXS experiments.

Experiments were conducted at beam line 5ID-D (DND-CAT) of the Advanced

Photon Source at Argonne National Laboratory. The x-ray energy was 15 keV,

corresponding to a wavelength $\lambda = 0.827$ Å. Two-dimensional SAXS patterns were

collected at a resolution of 1024 x 1024 pixels using an area detector (MarCCD) placed at

a sample-detector distance of 4.02 m. The image exposure time was 1 second, resulting

in a cycle time of 5 seconds per data frame when the image readout time is included. All

x-ray experiments were conducted at 130˚C.

To analyze SAXS patterns, quantitative scans of scattered intensity were first

extracted using the program Fit2D.[26] One-dimensional scans of $I(q)$ were extracted from

narrow sectors defined parallel and perpendicular to the stretching directions (here

$q = (4\pi / \lambda)\sin\theta$ is the magnitude of the scattering vector, where 2θ is the angle between

the incident and scattered beam). These scans were further analyzed to accurately

determine peak positions through a polynomial fit of $I(q)$ data near the peak. In addition,

azimuthal scans, $I(\phi)$, were extracted, integrating over a q-range encompassing the

primary diffraction peak (here ϕ is an azimuthal angle measured away from the stretching

direction). As described further below, such scans allow quantitative analysis of the

degree of microdomain orientation during and following extensional flow.

Results and discussion

The linear viscoelasticity measured at 130˚C in the melt of the SEBS triblock

copolymer shows enhanced low frequency elastic character typical of microphase

separated block copolymers (Fig. 1a). Data presented below confirm a hexagonally

ordered cylindrical morphology under these melt conditions. The high frequency regime

9

shows a rubbery plateau. Storage and loss moduli cross over as frequency is decreased, but rather than evolving towards the 'terminal' relaxation characteristic of viscoelastic liquids ($G' \sim \omega^2$, $G'' \sim \omega$), they cross over again such that G' again exceeds G'' at low frequency. Enhanced viscoelasticity at low frequencies is a robust signature of ordered morphologies in microphase-separated block copolymers, attributed to the elastic characteristics of the larger-scale ordered microdomains.[1,2] The viscoelastic relaxation time at the molecular scale may be estimated from the upper crossover frequency to be on the order of 1 second. Conversely, low-frequency viscoelasticity arising from the cylindrical ordering is associated with much longer relaxation times. At the extension rates used in this work, molecular viscoelasticity is expected by play a minor role; Weissenberg numbers based on the molecular relaxation time will be very small ($Wi = \lambda\dot{\varepsilon}$, where λ is the relaxation time and $\dot{\varepsilon}$ is the extension rate). However, these extension rates are more than sufficient to strongly perturb the larger-scale microphase-separated morphology.

We have performed additional linear viscoelastic testing to verify that our sample conforms to the thermal transitions reported in a similar SEBS triblock copolymer.[25] Upon heating to 150˚C, a sample that is initially conditioned to be in the cylindrical phase undergoes a slow order-order transition characterized by an increase in storage modulus and decrease in loss modulus. (Modi *et al.*[25] report that ~ 50 hours is required for this transition; see their Fig. 3. However, we find that this transition is completed in about half this time.)   After the transition, G' exhibits a robust, frequency-independent plateau at low frequencies, as found by Modi *et al.*, which was correlated with a transition to bcc

ordering of spherical microdomains.[25] Upon heating, a clear order-disorder transition is observed at 189°C (Fig.1b), as the elasticity associated with the ordered phase disappears.

Solid lines in Fig. 1a represent fits of a generalized Maxwell model with a discrete spectrum of relaxation times[27] to the linear viscoelastic data. In the limit of vanishing extension rate and/or small strains, the transient uniaxial extensional viscosity of viscoelastic fluids may be predicted from such linear viscoelastic data.[27] Despite the small extension rates employed here, strong deviations are observed between measurements of transient extensional viscosity in the SEBS triblock copolymer melt and corresponding linear viscoelastic predictions (Fig. 2). Data collected at different rates show considerable scatter at short times. We consider this primarily to be a consequence of the low extension rates used here. For instance, at 0.01 s^{-1}, an extensional strain of only 1% is achieved after 1 s of flow. Experimental data collected at short times using the SER fixture generally need to be corrected due to 'slack' developed in the sample because of thermal expansion upon heating into the melt. We have applied standard data correction procedures,[22,23] but the slow initial accumulation of extensional strain in these experiments nevertheless creates nonidealities during the early stages of deformation, leading to the variability seen in Fig. 2. The same issue presumably accounts for deviations between transient viscosity data and the linear viscoelastic predictions at short times for the lower extension rates.

At intermediate times, data collected at all three extension rates agree well with the linear viscoelastic prediction. At longer times, however, data deviate substantially from the prediction. Since it is expected that the polymer's microphase-separated structure will be strongly perturbed by the application of extensional flow, such

11

deviations are not surprising. At all three extension rates, the deviations occur at Hencky strains in the range of $0.1 - 0.2$. At larger strains the uniaxial viscosity remains roughly constant for the duration of the stretching. While transient extensional viscosity data in conventional polymer melts often show positive deviations from linear viscoelastic predictions (so-called 'strain-hardening'),[27] the opposite is observed here. A constant value of extensional viscosity implies that the tensile force (or, equivalently, engineering stress) in the deforming sample strip decreases as a function of time. Thus, the ordered SEBS melt may be considered to undergo a yielding transition[28] at a critical strain around 0.1 - 0.2. In the remainder of the paper, we employ *in situ* x-ray scattering to probe the microscopic structural changes that underlie and accompany this rheological behavior.

Two-dimensional SAXS patterns collected following inception of transient extensional flow reveal a complex structural response to the applied deformation (Fig. 3). SAXS data collected prior to flow show that the sought-for random distribution of domain orientation was not achieved in the samples studied here (Fig. 3a). The partial concentration of the primary SAXS peak intensity along the stretching direction indicates a weak bias in alignment of PS microdomains perpendicular to the stretching direction. Although the data of Fig. 1b confirm that the initial stage of sample sheet molding, at 200˚C, was conducted above the order-disorder transition of this polymer, this annealing step may have been of too short duration to fully erase orientation induced by the compression. Alternatively, it is also possible that some deformation took place during sample cooling, leading to the weak anisotropy observed in Fig. 3a.

Two distinct modes of structural response are observed upon inception of extensional flow. First, the primary diffraction ring in these 2D patterns is visibly

12

distorted, contracting along the stretching direction (horizontal), and elongating along the compression axis (vertical). Given the inverse relationship between real space and reciprocal space, this corresponds to an increase in microdomain spacing along the stretching axis, and reduction in spacing along the compression axis. Second, there is a complex reorientation process, whereby the initial concentration of diffracted intensity along the stretching direction is redistributed, eventually accumulating perpendicular to the stretching direction. Again, given the inverse character of reciprocal space, this corresponds to reorientation of elongated PS microdomains towards the stretching direction. This reorientation process is somewhat complex, as characteristic 'four-point' patterns are observed at intermediate times/strains during the stretching. Most of the reorientation process is completed relatively early in the experiment, within an applied Hencky strain of ~ 1. Continued stretching beyond this point does not produce further qualitative changes in the 2D SAXS patterns, although the scattered intensity continues to decrease owing to the exponentially decreasing sample thickness.

To study the flow-induced distortion of the microphase separated structure, one-dimensional $I(q)$ scans were extracted parallel and perpendicular to the stretching direction (see Fig. 3a). Fig. 4 presents examples of such scans extracted parallel to the stretching direction during the early stages of the same experiment for which representative images were presented in Fig. 3. Prior to flow inception, the quiescent data show clear evidence of hexagonal ordering, with two higher order diffraction peaks located at multiples $\sqrt{3}$ and $\sqrt{4}$ of the primary peak location, q^*. These results are in accord with observations of Modi and coworkers on a similar SEBS triblock polymer.[25] Upon inception of extensional flow, both primary and higher order diffraction peaks

initially shift towards smaller q, indicative of an increase in the d-spacing along the stretching direction. This trend does not continue, however. Rather, for Hencky strains greater than ~ 0.2, the primary peak reverses direction and begins to move out towards somewhat larger q values. At the same strain, higher order peaks become much less organized; it appears that the long range hexagonal ordering of PS microdomains is severely disrupted at this point.

The shifts in peak location may be quantified by extracting d-spacings (computed as $d = 2\pi/q^*$) associated with the primary diffraction peak observed in $I(q)$ scans taken in both parallel and perpendicular directions. Significant flow-induced distortion of microdomain structure is observed at all extension rates studied (Fig. 5a). Early in each experiment, d-spacings are observed to strongly increase and decrease along, respectively, the stretching and compression axes. As anticipated from the $I(q)$ scans in Fig. 4, this trend does not continue, and during much of the stretching process a roughly 'steady' degree of distortion is observed. When flow is stopped after an applied Hencky strain of 2.5, the flow-induced distortion relaxes very quickly: d-spacings measured parallel and perpendicular values again become equal. However, the d-spacing observed following flow cessation is significantly smaller (roughly 94%) than that present prior to flow. It is thus clear that the stretching process has led to significant changes in the microdomain organization in this material. Data collected in repeated experiments on fresh samples (open and closed symbols in Fig. 5) show excellent reproducibility.

Fig. 5b replots the d-spacing data, now normalized by their initial values and plotted as a function of the applied Hencky strain. At small strains, data collected at the different extension rates scale nearly perfectly with applied strain. The data are also in

14

quantitative agreement with predicted changes in *d*-spacing associated with affine

deformation of the microphase separated domain structure:

$$d^{\parallel} = d_0 \exp(\dot{\varepsilon}t), \tag{1a}$$

$$d^{\perp} = d_0 \exp(-\dot{\varepsilon}t / 2). \tag{1b}$$

The data break from the affine prediction at a Hencky strain of around 0.2. During

subsequent stretching, the 'steady' anisotropy in *d*-spacing increases with increasing $\dot{\varepsilon}$.

For instance, the value of $d^{\parallel} / d^{\perp}$ averaged over Hencky strains between 1 and 2

increases from 1.09 at $\dot{\varepsilon} = 0.01$ s^{-1} to 1.19 at $\dot{\varepsilon} = 0.05$ s^{-1}.

It is clear that there is a significant structural transition at Hencky strain ~ 0.2.

This transition is well correlated with the deviation of transient extensional viscosity data

from the linear viscoelastic prediction; thus, the 'yielding' observed in the mechanical

data (Fig. 2) is associated with this structural transition. Prior to this point, the persistence

of multiple higher order diffraction peaks confirms that hexagonal ordering remains

intact while the microphase separated structure is affinely deformed. Due to the

constraints of chain connectivity and packing, such affine deformation at the microscopic

scale cannot, of course, continue indefinitely. The break from the affine predictions, and

the suppression of higher order reflections observed at $\varepsilon_H \sim 0.2$ suggests that the long-

range order in the melt is severely disrupted at this point. Evidence of continued re-

orientation processes after critical strain indicates that the sample must still contain

elongated PS microdomains capable of being oriented by the flow. However, we do not

consider it likely that the microdomains continue to take the form of well-defined

cylinders after the yielding transition. Proximity of an order-order transition to a

spherical morphology suggests that initially cylindrical microdomains may be

particularly susceptible to break-up in this polymer. However, there is no evidence of formation of ordered arrays of spheres (e.g. higher order reflections characteristic of a bcc lattice), and disordered spherical microdomains would not be expected to yield significant anisotropy in scattering patterns. Thus, we conclude that the microscopic structure following yielding likely consists of elongated but disorganized PS microdomains that continue to orient towards the stretching direction. Such radical changes in microdomain morphology must also be accompanied by changes in the topology of polymer chains, in particular the relative fraction of loops vs. bridging chains, which could have consequences on the physical properties of products produced in processes which involve strongly extensional flow fields.

We turn next to investigation of the domain reorientation process. Since elongated microdomains produce diffraction perpendicular to their axes in reciprocal space, there is a mapping between azimuthal scans of scattered intensity, $I(\phi)$ [see Fig. 3e] and the underlying microdomain orientation distribution function. Azimuthal intensity scans show the initial bias in the grain orientation distribution (Fig. 6; here we only report $I(\phi)$ scans over the range [0, 180°] to avoid the shadow of the beam stop holder in the lower portion of the 2D SAXS patterns). Due to reciprocal relationships in scattering, the excess intensity in the horizontal direction ($\phi = 0$ or 180°) corresponds to a weak preferential alignment of hexagonally packed cylinder grains along the vertical direction, which, because of how specimens were cut, is perpendicular to the subsequent stretching axis. During application of extensional flow there is a general weakening in scattered intensity due to the progressive thinning of the sample strip. As flow proceeds, scattered intensity migrates towards the axis perpendicular to the flow direction ($\phi = 90°$),

16

corresponding to progressive rotation of elongated PS microdomains towards the

stretching direction. The '4-point' feature seen in 2D SAXS patterns is manifested as a

double peak in these scans. These two peaks in $I(\phi)$ eventually merge into a single peak

centered at $\phi = 90°$. During the later stages of the experiment, the relative magnitude of

this peak decreases. Fig. 6 also shows a comparison of azimuthal scans for the final

SAXS pattern collected prior to flow cessation and one collected 213 seconds following

flow cessation. In this case the average intensity remains constant since the sample

thickness is no longer changing. However, there is a clear relaxation in the degree of

microdomain orientation revealed by the increased isotropy in the azimuthal intensity

scan.

Changes in the degree of microdomain orientation may be compactly represented

through construction of a second moment tensor of the azimuthal intensity distribution.

Each point on the azimuthal scan may be represented by a unit vector $\mathbf{u} = (\cos\phi, \sin\phi)$

(Fig. 3e). For each SAXS pattern, the intensity-weighted average of the dyadic product

$\mathbf{uu}$ is computed as follows:[29]

$$\langle \mathbf{uu} \rangle = \begin{bmatrix} \langle \cos^2\phi \rangle & \langle \sin\phi\cos\phi \rangle \\ \langle \sin\phi\cos\phi \rangle & \langle \sin^2\phi \rangle \end{bmatrix} = \frac{\int_0^\pi \mathbf{uu}I(\phi)d\phi}{\int_0^\pi I(\phi)d\phi}. \tag{2}$$

As in the presentation of Fig. 6 we only used data in the range [0, 180°] in computing

$\langle \mathbf{uu} \rangle$ to avoid interference from the shadow of the beam stop holder. The normalization

in the denominator of the right hand side of Eq. (2) accounts for the changes in the

overall scattering power over the course of the experiment. Due to the symmetry of the

applied flow, the off-diagonal $\langle \sin\phi\cos\phi \rangle$ terms should be zero, and the degree of

orientation may be simply represented as the difference in the diagonal elements of $\langle \mathbf{uu} \rangle$,

which we call the 'anisotropy factor' or *AF*. Accounting for the reciprocal relationship

between orientation in real space and reciprocal space, we compute this as:

$$AF = \langle u_2 u_2 \rangle - \langle u_1 u_1 \rangle = \langle \sin^2 \phi \rangle - \langle \cos^2 \phi \rangle. \qquad (3)$$

Defined in this way, $AF = 0$ for the case of an isotropic scattering pattern with $I(\phi) =$

constant, while *AF* would equal 1 for the hypothetical case in which all scattered intensity

is perfectly concentrated at $\phi = 90°$, indicative of complete microdomain orientation

along the flow direction.

Fig. 7 presents results of this analysis procedure for experiments at the three

extension rates used here. Due to the initial bias in microdomain orientation, *AF* takes on

small negative values prior to flow, which vary somewhat from sample to sample. Upon

inception of extensional flow at all rates, the anisotropy increases rapidly, passes through

a maximum and then decreases as stretching continues. Upon flow cessation (after

application of 2.5 Hencky strain units), the anisotropy factor relaxes towards isotropy.

As with the *d*-spacing data presented earlier, repeated experiments demonstrate the

reproducibility of the orientation response.

Plotting anisotropy data during flow as a function of Hencky strain demonstrates

that the domain reorientation process is primarily governed by the applied strain, and,

over the range of rates used here, largely independent of the extension rate (Fig. 8a). At

all $\dot{\varepsilon}$, microdomain orientation reaches a maximum value at $\varepsilon_H \sim 1$, and decreases

thereafter. The decrease in anisotropy in the later stages of these experiments seems

counterintuitive. However, this may be rationalized as another manifestation of an

increasingly disorganized microdomain structure as the severe deformation associated

with extensional flow continues. In particular, the flow may lead to continued break-up of the elongated PS microdomains into smaller pieces, resulting in the reduction in microdomain orientation seen at long times. Interestingly, anisotropy factor data show no observable consequence of the abrupt structural transition that is apparent in d-spacing data at $\varepsilon_H \sim 0.2$. Similarly, the maximum in microdomain orientation at $\varepsilon_H \sim 1$ is not correlated with any discernable feature in the mechanical response.

The time scale of orientation relaxation is also largely independent of extension rate over this range (Fig. 8b). Relative to the very rapid relaxation in d-spacing upon flow cessation (Fig. 5a), the relaxation of AF is considerably slower, again demonstrating that these two modes of structural response—deformation and orientation—are significantly decoupled from one another.

Figures 5b and 8 show that many quantitative aspects of the structural response of this triblock copolymer melt to extensional flow are primarily governed by applied strain rather than extension rate. However, there are significant qualitative differences in SAXS patterns collected during experiments at different rates (Fig. 9). For a given degree of extension, the various scattering features are noticeably sharper at higher extension rates. Thus, for instance, at an intermediate Hencky strain of about 0.65, the 4-spot feature has already merged into a single broad peak at $\dot{\varepsilon} = 0.01$ s^{-1}, but is very much in evidence at $\dot{\varepsilon} = 0.05$ s^{-1}.

In situ scattering studies of structure during mechanical deformation of cylindrically ordered block copolymers in the *solid* state have frequently shown similar 4-point patterns in pre-aligned samples in which stretching is orthogonal to the orientation of cylindrical microdomains, such that the cylinders are subjected to compression.[4-6] The

prevailing hypothesis is that a buckling instability in the cylindrical microdomains creates a 'chevron' texture with two distinct populations of microdomain orientation which then re-orient towards the stretching direction. We postulate that a similar mechanism is responsible for the emergence of the 4-point patterns in these melt studies. Evidently, additional structural relaxation processes are present in the melt that lead to the more pronounced 'blurring' of these features at low rates, where the relative strength of the convective deformation driving the buckling and re-orientation processes is reduced.

Once the two populations of microdomain orientation are established, it is possible to track the rate at which they re-orient towards the stretching axis in terms of the angle β defined in Figs. 3d and 6, which indicates the degree of misalignment from the stretching direction. Over the portion of the experiments in which a distinct 4-point pattern is observed, the angle β is largely, although not solely, determined by the applied Hencky strain (Fig. 10). There is a small but systematic shift in the data towards larger Hencky strain as extension rate increases; that is, reorientation of these distinctive populations is somewhat retarded at higher extension rates. In light of the increased 'sharpness' of the corresponding 2D patterns at higher rates (Fig. 9), it is possible that more coherent defect structures (such as domain walls) are produced by the buckling instability in experiments at higher rates, which exert a stronger force resisting grain reorientation. Interestingly, however, the more global measure of microdomain orientation considered in Fig. 8a does not show a similar retardation of the rate of alignment with increasing extension rate.

Data in Fig. 10 may be benchmarked against a simple model of microstructure alignment under flow:[30]

$$\frac{\partial \mathbf{n}}{\partial t} = \mathbf{n} \cdot \nabla \mathbf{v} - \mathbf{nnn} : \mathbf{D} .$$ (4)

Here $\mathbf{n}$ is a unit vector indicating, in this application, the local microdomain orientation direction, $\nabla \mathbf{v}$ is the velocity gradient tensor, and $\mathbf{D}$ is the rate of deformation tensor (*i.e.,* the symmetric part of $\nabla \mathbf{v}$). The first term on the right side of Eq. (4) represents affine deformation, while the second term subtracts off the 'stretching' portion such that $\mathbf{n}$ remains a unit vector. This equation arises in the hydrodynamics of dilute suspensions of infinitely narrow rigid rods, and also governs orientation dynamics in the independent alignment version of the Doi-Edwards tube model, both of which involve orientation but no stretching.[30] In shear deformations, Eq. (4) is identical to the grain rotation model explored by Polis *et al.*[31] in studies of lamellar block copolymers in shear.

In uniaxial extensional flow, Eq. (4) predicts that a 'grain' initially oriented at an angle β_0 relative to the stretching axis will reorient according to:

$$\frac{\tan \beta}{\tan \beta_0} = e^{-\frac{3\dot{\varepsilon}t}{2}} .$$ (5)

As seen in Fig. 10, this simple affine reorientation model does a reasonable job capturing the experimentally observed behavior. Since it is hard to imagine a type of dynamics that would result in more a rapid reorientation of microstructure, one would expect Eq. (5) to bound the data from one side; this appears to be the case. [It is important to note that Eq. (4) is unable to account for the initial emergence of the discrete populations of microdomain orientation revealed by the 4-point SAXS pattern. Given an initially random orientation distribution of microdomains, Eq. (4) would only predict the monotonic growth of a single peak in the grain orientation distribution function, centered on the stretching direction.]

Conclusions

We have reported the first *in situ* scattering studies of extensional flow-induced structural changes in block copolymer melts. In the cylindrically ordered SEBS triblock copolymer sample studied here, x-ray scattering patterns reveal two distinct modes of structural response during extensional flow: deformation of the microscopic structure, and re-orientation of PS microdomains towards the flow direction. Until Hencky strains of around 0.2, *d*-spacings of the hexagonally ordered domains measured parallel and perpendicular to the flow direction deform affinely, and higher order reflections remain intact, indicating preservation of long-range order. Beyond this critical strain higher-order reflections are lost, and the flow-induced deformation of the structure no longer follows affine deformation, settling rather into a nearly steady value. The *d*-spacings relax quickly upon cessation of flow, although to a value considerably different than that initially observed. These observations suggest that considerable disruption in long-range ordering occurs at a critical strain of ~ 0.2, which also corresponds to the point at which transient extensional viscosity deviate strongly from linear viscoelastic predictions.

The aziumuthal dependence of the primary diffraction peak reveals a complex re-orientation process by which cylindrical PS microdomains orient towards the stretching direction. The re-orientation proceeds through an intermediate state in which a '4-point' diffraction pattern reveals the presence of two discrete populations of microdomain orientation. By analogy with similar previous observations of cylindrical block copolymers in the *solid* state, we speculate that this behavior emerges as a consequence of a compression-induced buckling instability of PS microdomains initially oriented

22

perpendicular to the stretching directions. An average measure of the overall degree of microdomain orientation passes through a maximum at an intermediate Hencky strain of around 1. The transient evolution of overall microdomain orientation is largely controlled by applied strain, independent of extension rate, although the 4-point patterns are considerably sharper at high rates. Upon flow cessation, relaxation in the degree of microdomain orientation is observed, although on a much longer time scale than the relaxation of flow-induced deformation of d-spacing. Thus, it appears that these two modes of structural response (deformation and domain re-orientation) are significantly decoupled.

Acknowledgments

References

1. I. W. Hamley, *The Physics of Block Copolymers*, Oxford University Press, New York, 1999.

2. R. G. Larson, *The Structure and Rheology of Complex Fluids*, Oxford University Press, New York, 1998.

3. I. W. Hamley, *J. Phys.: Condens. Matter,* 2001, **13**, R643-R671.

4. T. Pakula, K. Saijo, H. Kawai and T. Hashimoto, *Macromolecules*, 1985, **18**, 1294-1302.

5. C. C. Honeker and E. L. Thomas, *Chem. Mater*., 1996, **8**, 1702-1714.

6. C. C. Honeker, E. L. Thomas, R. J. Albalak, D. A. Hajduk, S. M. Gruner and M. C. Capel, *Macromolecules*, 2000, **33**, 9395-9406.

7. P. Kofinas and R. E. Cohen, *Macromolecules,* 1995, **28**, 336-343.

8. D. B. Scott, A. J. Waddon, Y.-G. Lin, F. E. Karasz and H. H. Winter, *Macromolecules*, 1992, **25**, 4175-4181.

9. H. H. Lee, R. A. Register, D. A. Hajduk and S. M. Gruner, *Polym. Eng. Sci.,* 1996, **36**, 1414-1424.

10. C. Daniel, I. W. Hamley and K. Mortensen, *Polymer,* 2000, **41**, 9239-9247.

11. J. Meissner and J. Hostettler, *Rheol. Acta,* 1994, **33**, 1-21.

12. T. Takahashi, J.-I. Takimoto, and K. Koyama, *J. Appl. Polym. Sci.,* 1998 **69**, 1765-1744.

13. T. Kotaka, M. Okamoto, A. Kojima, Y. K. Kwon and S. Nogima, *Polymer,* 2001, **42**, 1207-1217.

14. T. Kotaka, M. Okamoto, A. Kojima, Y. K. Kwon and S. Nogima, *Polymer,* 2001, **42**, 3223-3231.

15. Y. Kobori, Y. K. Kwon, M. Okamoto and T. Kotaka, *Macromolecules,* 2003, **36**, 1656-1664.

16. Y. K. Kwon, Y. S. Ko and M. Okamoto, *Polymer,* 2008, **49**, 2334-2341.

17. H. M. Laun and J. Munstedt, *Rheol. Acta,* 1976, **15**, 517-524.

18. H. Munstedt and H. M. Laun, *Rheol. Acta,* 1981, **20**, 211-221.

19. A. Bach, K. Almdal, H. K. Rasmussen and O. Hassager, *Macromolecules,* 2003, **36**, 5174-5179.

20. H. K. Rasmussen, J. K. Nielsen, A. Bach and O. Hassager, *J. Rheol.*, 2005, **49**, 369-381.

21. J. Meissner, T. Raible and S. E. Stephenson, *J. Rheol.*, 1981, **25**, 1-28.

22. M. L. Sentmanat, *Rheol. Acta,* 2004, **43**, 657-669.

23. M. Sentmanat, B. N. Wang and G. H. McKinley, *J. Rheol.*, 2005, **49**, 585-606.

24. K. Yu, J. M. R. Marin, H. K. Rasmussen and O. Hassager, *J. Non-Newtonian Fluid Mech.,* 2010, **165**, 14-23.

25. M. A. Modi, R. Krishnamoorti, M. F. Tse and H.-C. Wang, *Macromolecules*, 1999, **32**, 4088-4097.

26. A. Hammersley, web source: http://www.esrf.eu/computing/scientific/FIT2D/.

27. C. W. Macosko, *Rheology: Principles, Measurements and Applications*, VCH, New York, 1993.

28. G. Liu, H. Sung, S. Rangou, K. Ntetsikas, A. Avgeropoulos and S.-Q. Wang, *J. Rheol.*, 2013, **57**, 89-104.

29. D. K. Cinader and W. R. Burghardt, *J. Polym. Sci.: Part B Polym. Phys.*, **1999**, 37, 3411-3428.

30. R. G. Larson, *Constitutive Equations for Polymer Melts and Solutions, Butterworths*, Stoneham MA, 1988.

31. D. L. Polis, S. D. Smith, N. J. Terrill, A. J. Ryan, D. C. Morse and K. I. Winey, *Macromolecules*, 1999, **32**, 4668-4676.
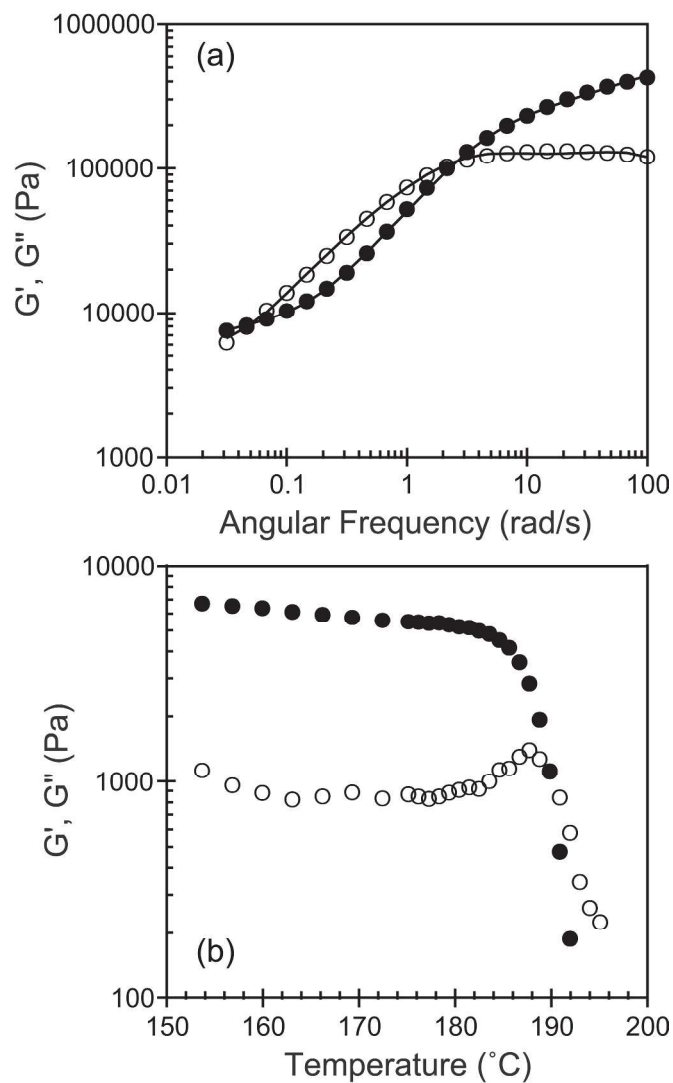
Fig. 1 Rheology of SEBS triblock copolymer melt. (a) Linear viscoelasticity measured at 130˚C: (●) storage modulus, and (○) loss modulus. Lines represent predictions of a multimode Maxwell model fit to the data. Under these conditions, the sample adopts a hexagonally-packed cylinder morphology. (b) Temperature ramp experiment performed at angular frequency $\omega = 0.03$ rad/s, after prolonged annealing at 150˚C to produce an ordered spherical microphase-separated morphology. The abrupt drop in G' confirms an order-disorder transition at 189 ˚C. The heating rate was 0.3 ˚C from 150 to 175 ˚C, and 0.1 ˚C/min from 75 to 200 ˚C.
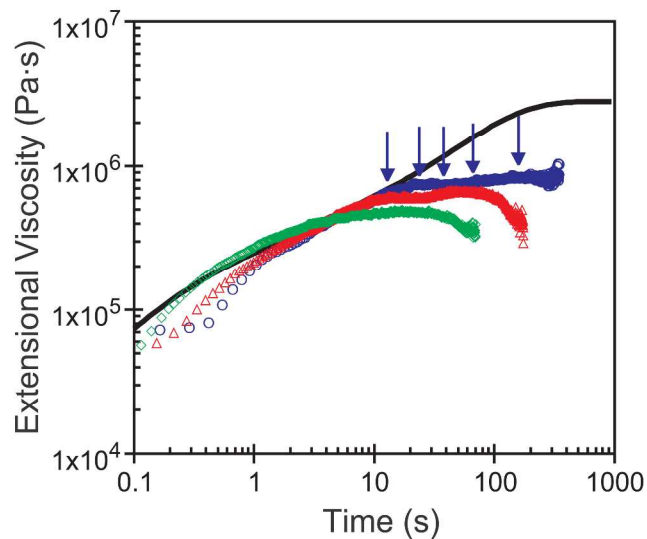
Fig. 2 Transient uniaxial extensional viscosity measured in SEBS triblock copolymer sample at 130˚C using extension rates of 0.01 (○), 0.02 (△) and 0.05 s^{-1} (◇). Solid curve represents linear viscoelastic prediction, using the Maxwell model fit to data in Figure 1. Arrows indicate time points for which SAXS images are presented in Fig. 3, below.

28
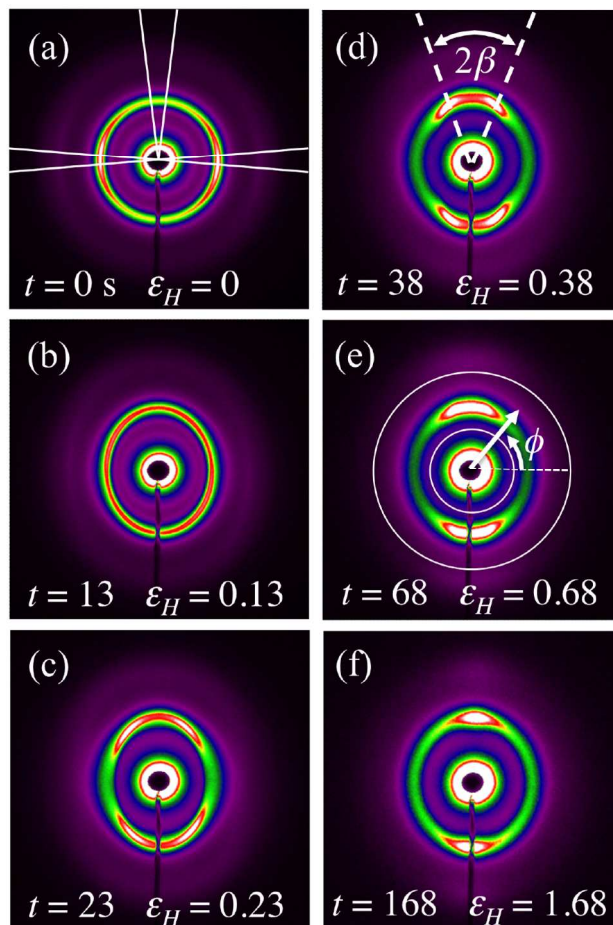
Fig. 3 Two-dimensional SAXS patterns measured in SEBS triblock copolymer melt at indicated time/Hencky strain during inception of uniaxial extensional flow at an extension rate of 0.01 s^{-1} and temperature of 130°C. The primary stretching direction is horizontal. Overlays in part (a) illustrate sectors used to extract $I(q)$ data parallel and perpendicular to the stretching direction. Overlays in part (d) illustrate definition of angle β used to characterize the 'double-peak' feature observed at intermediate times. Overlays in part (e) define the q-range over which azimuthal intensity scans, $I(\phi)$, are extracted.
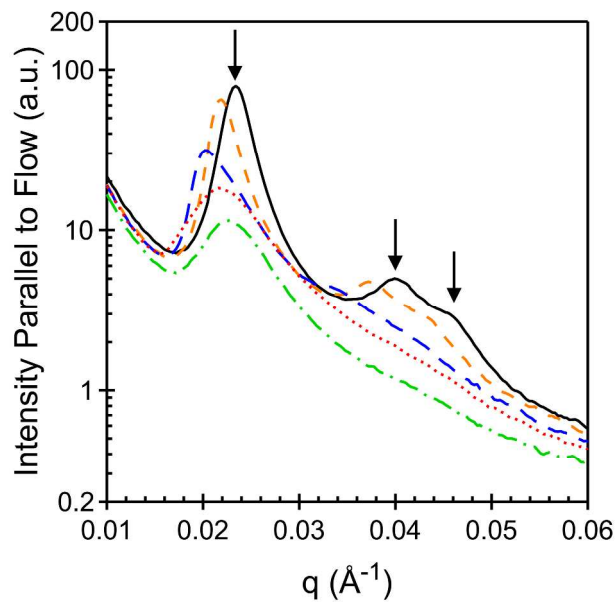
Fig. 4 Evolution of $I(q)$, measured parallel to the stretching direction, during inception of uniaxial extensional flow at a rate of 0.01 s^{-1}. Data presented at $t = 0$ s, $\varepsilon_H = 0$ (———); $t = 8$ s, $\varepsilon_H = 0.08$ (- - -); $t = 18$ s, $\varepsilon_H = 0.18$ (– – –); $t = 28$ s, $\varepsilon_H = 0.28$ ($\cdots\cdots$); and $t = 68$ s, $\varepsilon_H = 0.68$ (– · – · –). Arrows indicate peak spacing expected for hexagonal ordering of cylindrical domains: $q^*, \sqrt{3}q^*, \sqrt{4}q^*$.

30
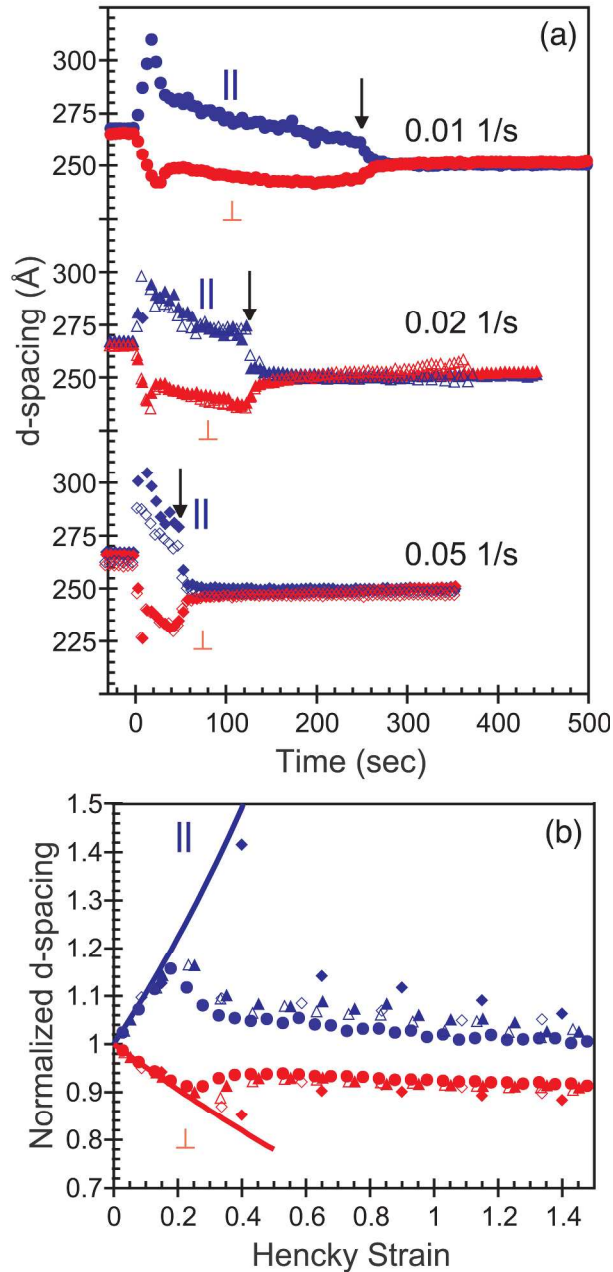
Fig. 5 Microscopic deformation of ordered triblock copolymer melt during inception of transient extensional flow at rates of 0.01 (●), 0.02 (▲,△) and 0.05 s^{-1} (◆,◇). Open and closed symbols represent results of duplicate experiments under identical conditions. (a) Microdomain *d*-spacing associated with primary SAXS peak measured parallel (∥) and perpendicular (∞) to the stretching direction as a function of time. Arrows indicate the point of flow cessation, at $\varepsilon_H = 2.5$. (b) Normalized *d*-spacing measured at short times plotted as a function of applied Hencky strain, ε_H. Lines represent predictions of affine deformation model, eqs. (1).
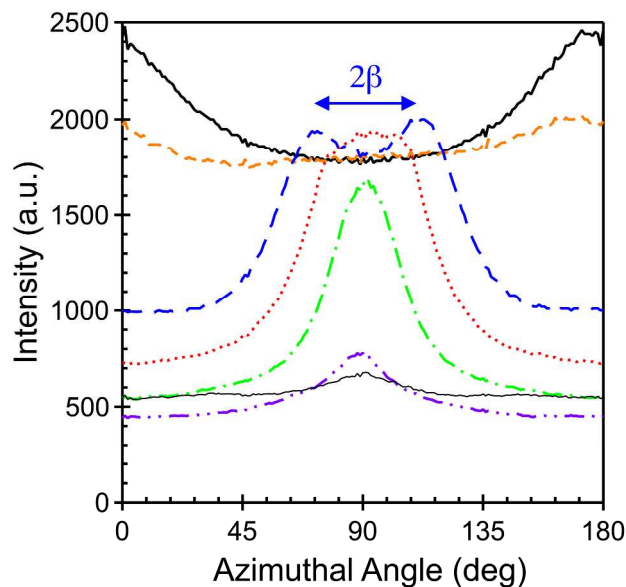
Fig. 6 Azimuthal intensity scans, $I(\phi)$, extracted from SAXS patterns collected during inception of uniaxial extensional flow at a rate of 0.01 s^{-1}. Data presented at $t = 0$ s, $\varepsilon_H = 0$ (———); $t = 8$ s, $\varepsilon_H = 0.08$ (- - -); $t = 38$ s, $\varepsilon_H = 0.38$ (– – –); $t = 68$ s, $\varepsilon_H = 0.68$ ($\cdots\cdots$); $t = 118$ s, $\varepsilon_H = 1.18$ (– $\cdot$ – $\cdot$ –); and $t = 248$ s, $\varepsilon_H = 2.48$ (– $\cdot\cdot$ – $\cdot\cdot$ –). The thin solid curve represents data measured 213 s following flow cessation.
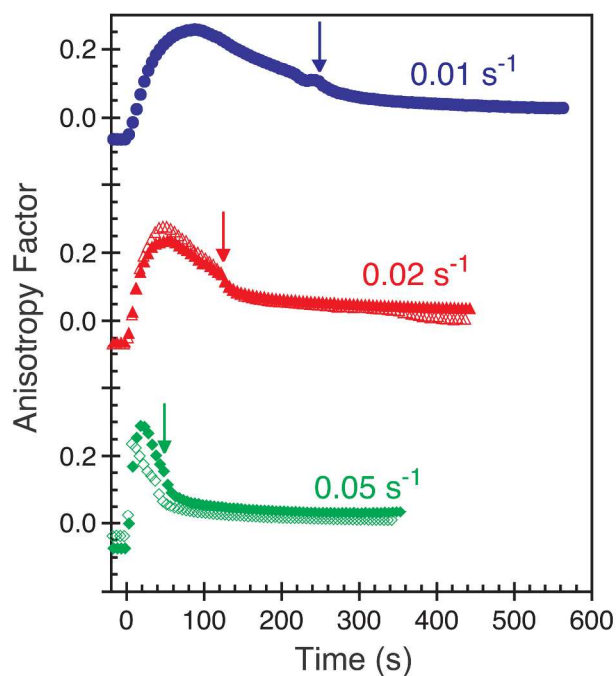
Fig. 7 Microdomain reorientation (anisotropy factor vs. time) measured in ordered triblock copolymer melt during inception and following cessation of transient extensional flow at rates of 0.01 (●), 0.02 (▲,△) and 0.05 s^{-1} (◆,◇). Open and closed symbols represent results of duplicate experiments under identical conditions. Arrows indicate the point of flow cessation, at $\varepsilon_H = 2.5$.
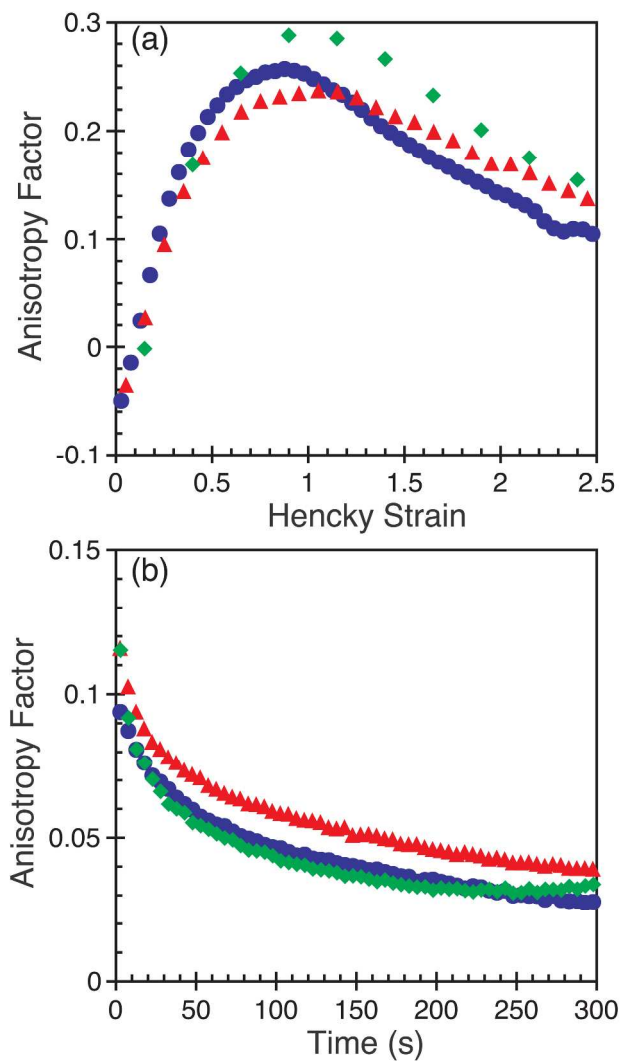
Fig. 8 Impact of extension rate on microdomain reorientation process. Anisotropy factor plotted as a function of (a) Hencky strain during uniaxial extensional flow, and (b) time following flow cessation, at rates of 0.01 ($\bullet$), 0.02 ($\blacktriangle$) and 0.05 s^{-1} ($\blacklozenge$).
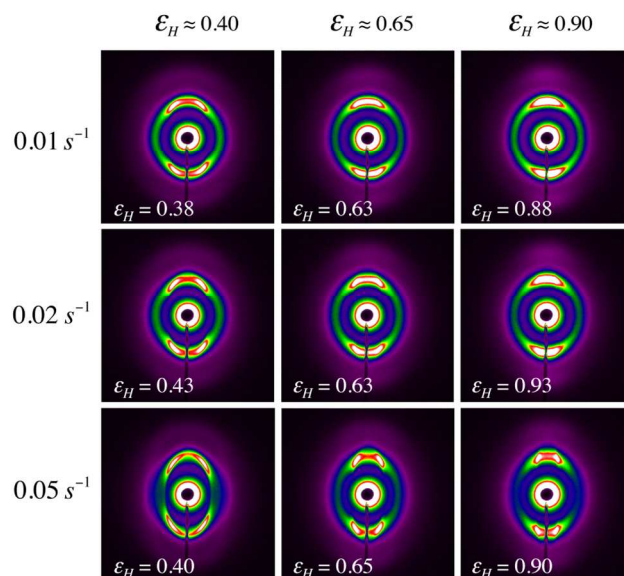
Fig. 9 Qualitative impact of extension rate on two-dimensional SAXS patterns measured at three representative (nominal) strains during inception of uniaxial flow at indicated rates. (Due to limitations on data acquisition rate, it was not possible to extract images at precisely the same Hencky strains for experiments at the different extension rates. The exact Hencky strain is reported for each image.)
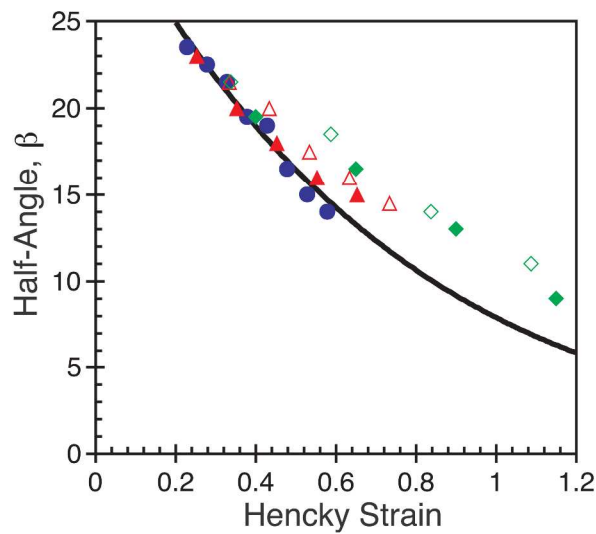
35

Fig. 10 Evolution of 'double-peak' feature during during inception of transient extensional flow at rates of 0.01 (●), 0.02 (▲,△) and 0.05 s^{-1} (◆,◇). Half-angle β, defined in Figures 3 and 6, is plotted as a function of applied Hencky strain. Open and closed symbols represent results of duplicate experiments under identical conditions. Solid line is prediction of affine orientation model, Eq. (5).